Available online at www.sciencedirect.com
ScienceDirect
Journal of Nuclear Materials 363–365 (2007) 78–85
journal of nuclear materials
www.elsevier.com/locate/jnucmat

Modeling of asymmetric redeposition distribution between inner and outer regions of the W-shaped divertor in JT-60U

K. Ohya [a,*], K. Inai [b], T. Tanabe [c], H. Takenaga [d]

[a] *Institute of Technology and Science, The University of Tokushima, Minamijosanjima 2-1, Tokushima 770-8506, Japan*
[b] *Graduate School of Advanced Technology and Science, The University of Tokushima, Tokushima 770-8506, Japan*
[c] *Interdisciplinary Graduate School of Engineering Science, Kyushu University, Fukuoka 812-8581, Japan*
[d] *Fusion Research and Development Directorate, Japan Atomic Energy Agency, Ibaraki 311-0193, Japan*

Abstract

Poloidal distributions of erosion depth and deposition thickness on components in the inner and outer regions of the W-shaped divertor in JT-60U are modeled using EDDY. Hydrocarbons released from the outer divertor plate are immediately ionized when entering the plasma and are redeposited near the release position. But they are subjected to re-erosion by the successive bombardment of plasma ions, resulting in small effective sticking. On the whole, most area of the outer divetor plate are eroded agreeing with observed distributions of erosion depth. In contrast, the inner divertor plate is dominated by deposition and the observed poloidal distribution of the thickness of the redeposited carbon layers agrees with incoming carbon flux from the plasma without re-erosion owing to lower-temperature. Due to much lower-temperature ($\sim$1 eV) of the private plasma in the outer region, the neutral carbon/hydrocarbon species are locally redeposited at the bottom edge of the outer dome wing adjacent to the bottom of the outer divertor plate.

PACS: 52.40.Hf; 52.55.Fa; 52.55.Rk; 52.65.Pp

Keywords: Co-deposition; Divertor; Edge modeling; Erosion and deposition; Hydrocarbons; JT-60U

1. Introduction

Tritium retention is a critical problem for next-step fusion reactors with carbon plasma-facing components. In present large tokamaks, most of the hydrogen isotopes are retained in the carbon deposition layers on the components in the divertor. Recently, the deposition profile and hydrogen retention in large tokamaks [1–4] were found to be dependent on the structure of the divertor, including the asymmetry between inner and outer regions. Erosion was dominant on the outer divertor plate, whereas deposition was dominant on the inner plate. Furthermore, modeling studies using impurity transport codes, such as WBC code [5] and ERO code [6] were done for the erosion and redeposition on the divertors of the present tokamaks and ITER [7–9]. Localized heavy deposition has also recently

* Corresponding author. Tel./fax: +81 886 56 7444.
E-mail address: ohya@ee.tokushima-u.ac.jp (K. Ohya).

0022-3115/$ - see front matter
doi:10.1016/j.jnucmat.2006.12.061

been observed in the private flux region of the W-shaped divertor in JT-60U [10], in which the outer dome wing plate was mostly covered by deposition. The heaviest deposition was observed on the underside of the wing that did not directly face the plasma. In the present study, we modeled hydrocarbon transport in the inner and outer regions of the W-shaped divertor in JT-60U with a simulation code, EDDY, and investigated the redeposition mechanism of carbon and hydrocarbons in divertor area and the origin of the in–out asymmetry in erosion and deposition patterns.

2. Divertor model and experimental condition used for calculation

For the simulation, we used true-size divertor plates and dome wings from the inner and outer regions of the W-shaped divertor. Fig. 1 shows a schematic view of the divertor, along with the variation of plasma parameters with the poloidal distance. The plasma parameters above the diverter plates were calculated using the 2D fluid divertor code UEDGE with an ion density of 10^{19} m^{-3} and a power flow of 8 MW at the core boundary [11]. The plasma ion and electron temperatures in the divertor were lower for the detached inner region than for the attached outer region. Each point on the divertor plates was bombarded by the plasma hydrogen ions that contain carbon impurities of ~2% and 0.7% at the strike points for the inner and outer regions, respectively, these values also depend on the positions on the plates. The magnetic field strength was 3 T and 2.7 T in the inner and outer divertor plates, respectively, while for both plates the angle of the magnetic field line to the toroidal direction was 2°.

The erosion and redeposition patterns on the plates were calculated using EDDY [12], which treats transport of impurities released from the plates in the plasma. The code also simulates dynamic material mixing processes, which is a main difference from other impurity transport codes [5,6]. Furthermore, energy-dependent reflection and dissociation of hydrocarbons on the surface was employed in addition to a well-used constant sticking coefficient, S_{div}, of each hydrocarbon on the plate. For the chemical erosion of the carbon

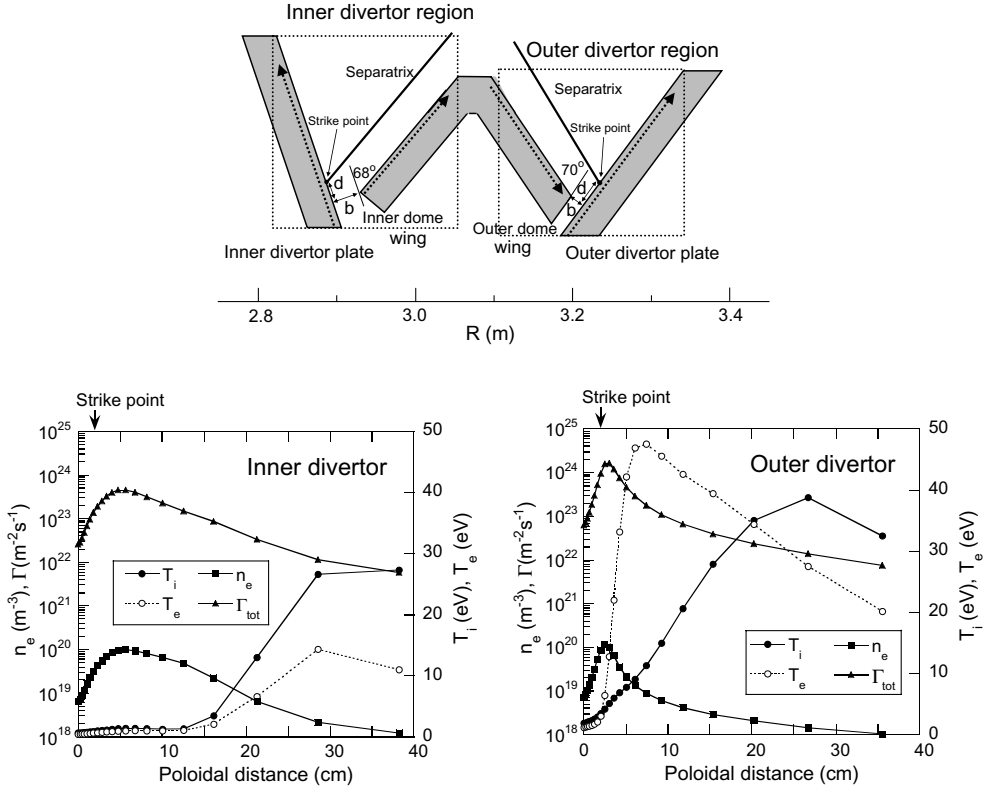

Fig. 1. Schematic view of the W-shaped divertor geometry in JT-60U and plasma parameters used for simulation.

divertor plates, only a methane molecule (CH_4) was assumed to be released according to the chemical sputtering yield; the formation of higher hydrocarbons was not taken into account. For physical sputtering, only carbon atoms were released. The released carbon atoms and hydrocarbons were ionized or dissociated via collisions with plasma electrons and ions. The CH_4 molecules were subjected to complex dissociation reactions than simple ionization of carbons. According to a new set of fitting formulae taken from Janev and Reiter [13] for the rate coefficients of the collisional (dissociation and/or ionization) reactions, which was used in the ERO code [6], various neutral and ionized fragments are produced via successive reaction chains. The collisional transport processes were followed by combining kinetic equation analysis and Monte-Carlo simulation, which are basically similar to other transport codes [5,6]. In this study, when a particle produced by the reaction is charged, it gyrates in the plane perpendicular to the magnetic field line. The equation of motion with the velocity, $v_{||}$, parallel to the field line is

$$m\frac{\mathrm{d}v_{||}}{\mathrm{d}t} = m\frac{v_{||} - v_{\mathrm{p}}}{\tau_{\mathrm{s}}} + \alpha\frac{\mathrm{d}T_{\mathrm{e}}}{\mathrm{d}s} + \beta\frac{\mathrm{d}T_i}{\mathrm{d}s}. \quad (1)$$

The first term in the right hand side is the friction force, whereas the second and third terms are the thermal gradient force as described in Ref. [14]. Furthermore, we take into account the anomalous diffusion across the field lines, which was taken from Shimizu et al. [15], the sheath and presheath acceleration towards the plates with the so-called Brooks parameter [16] and the elastic collisions with the residual neutral hydrogen by the hard sphere collision model [17]. Before the charging, particles move along straight lines, but they are suffered by elastic collisions. Although carbon impurities originating from the outer region are not directly taken into account as deposition source at the inner divertor plate, the effect is taken into account as higher carbon concentration in the inner divertor plasma (~2% at the strike point) than that for the outer divertor plasma (0.7%). In the simulation, therefore, carbon is eroded by physical and chemical sputtering of hydrogen plasma ions and physical sputtering of carbon impurity ions, while it is deposited as impinging of plasma carbon impurities and local redeposition (or prompt redeposition) of sputtered carbons and hydrocarbons. Areas on the divertor plates and dome wings are divided into numerous segments in the poloidal direction; a symmetry is assumed in the toroidal direction to enable the carbon/hydrocarbon release and erosion and deposition patterns to be calculated in each segment. Some particles redeposit promptly on the same segment from which they were released, or redeposit on another segment after migration in the plasma.

The calculated results are compared with the erosion and redeposition patterns on the divertor plates, which were exposed to ~4300 discharges in the 1997–1998 experimental campaigns [4]. Since, in JT-60U, various kind of discharges with different plasma parameters and different discharge times were performed, the erosion and redeposition patterns on the surface of the divertor plates obtained by the postmortem analysis were superposition of the patterns given by each discharge. Therefore, erosion and redeposition patterns calculated for a single discharge with a fixed discharge time (10 s) and a typical plasma distribution (Fig. 1) were convoluted with strike point distributions (upper figures in Fig. 2) according to the real distribution [4] on the divertor plates in the poloidal direction, resulting in the erosion depth and deposition thickness given in Fig. 2.

3. Results and discussion

The bombardment of carbon materials with a hydrogen plasma that contains carbon impurities causes simultaneously erosion and deposition, which are, respectively, caused by chemical and physical sputtering and by deposition of hydrocarbons produced by chemical sputtering and impinging of impurity carbon. Multiply ionized carbon atoms in the background plasma were accelerated by the sheath toward the surface resulting in higher sticking. On the other hand, most of eroded carbon atoms and hydrocarbons are immediately ionized and returned near the eroded location without appreciable acceleration by the sheath, and hence their impinging energies are low and significant amount carbon atoms are reflected. The sticking coefficient, S_{div}, for hydrocarbons on the surface varies from $S_{\mathrm{div}} = 1$, i.e. all hydrocarbons being stuck and deposited on the plate without reflection to $S_{\mathrm{div}} = 0$, i.e. no sticking or full reflection, depending on impinging particle species and energies, and the surface conditions such as temperature and roughness. For $S_{\mathrm{div}} = 0$, only plasma carbon impurities remains as deposition source. Unfortunately, qualitative dependence of the sticking coefficient

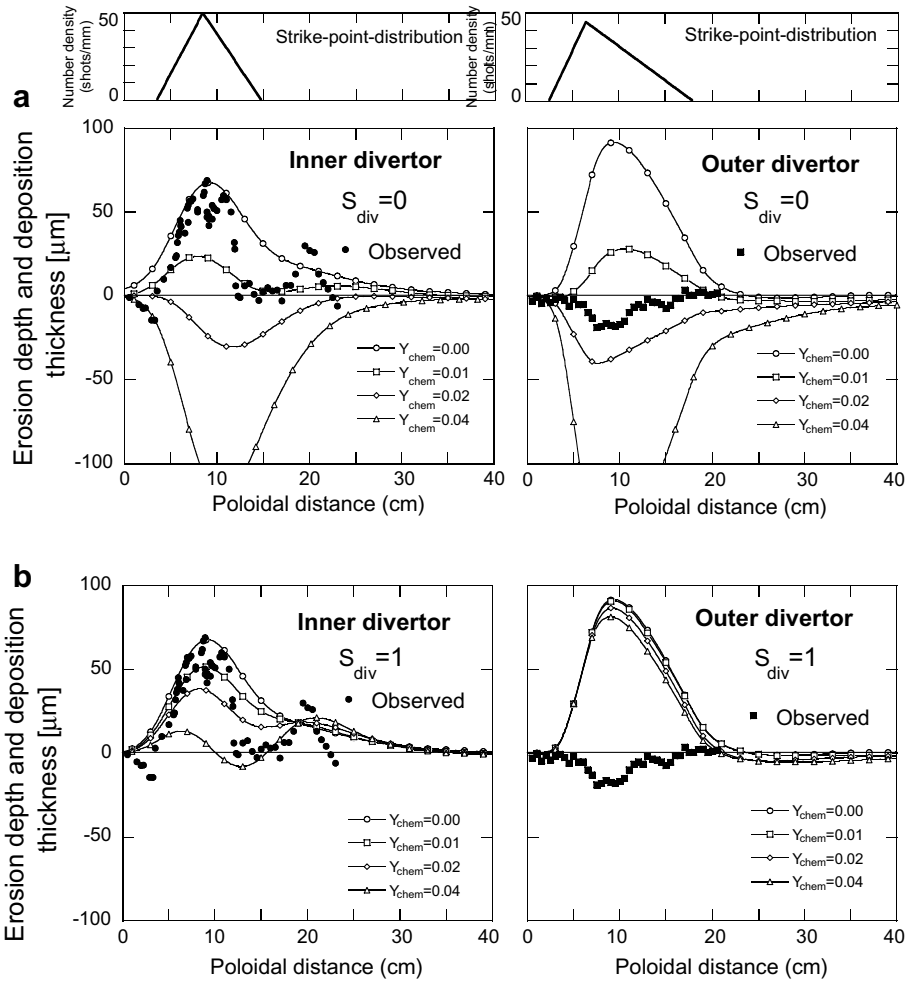

Fig. 2. Poloidal distribution of deposition layer thickness and erosion depth on the inner and outer divertor plates as a function of the chemical sputtering yield (Y_{chem}) and the sticking coefficient (S_{div}). Solid symbols correspond to the observed deposition layer thicknesses and erosion depths published by Gotoh et al. [4]. Upper figures correspond to strike point distributions modeled on the divertor plates for the 1997–1998 experimental campaigns.

on these parameters are available until now. Here, therefore, the erosion and deposition patterns on the divertor plates in the inner and outer regions were calculated as a function of the sticking coefficient and chemical sputtering yield as shown in Fig. 2. The patterns with no chemical erosion ($Y_{chem} = 0$) correspond to the distribution of the background carbon deposition, except for the poloidal distances greater than 25 cm on the outer divertor target; in this case, the deposited carbon is eroded only by physical sputtering. Although physical sputtering causes the erosion near the strike point on the outer divertor plate, the prompt redeposition related to the high density of plasma in front of the plate substantially decreases the erosion depth. For zero sticking ($S_{div} = 0$), the increase of the chemical sputtering yield results in dominating the erosion at both the inner and outer divertor plates. For full sticking ($S_{div} = 1$), due to higher temperature of the plasma over most of the area of the outer plate, many hydrocarbons eroded from the outer plate are promptly redeposited, so that the deposition still dominates the distribution. Reasonable agreement with the observed erosion distribution [4] in the poloidal direction is achieved only via the assumption of negligible effective sticking of hydrocarbons and an effective chemical sputtering yield of 0.01–0.02 on the outer divertor plate. The discharge analyzed in the present study is not representative of all the discharges during the experimental campaign of JT-60U. Although this low sticking coefficient on the outer divertor plate must

be checked via comparisons with future experiments, one possible explanation for the low sticking is the repeated erosion and redeposition associated with successive bombardments of the redeposited surface with high-fluence plasma hydrogen ions.

The poloidal distribution of the observed thickness of the carbon deposition layer on the inner divertor plate is explained by both the deposition of carbon impurities in the background plasma and the redeposition of hydrocarbons released from the surface. The preferential deposition of carbon impurities on the inner divertor plate is due to higher carbon concentration (~2% at the strike point) for the inner divertor region than for the outer region (~0.7%), which itself is a consequence of the SOL flow or drift flow from the outer divertor region to the inner region via the private flux region [18]. The effective chemical sputtering yield (or the effective sticking coefficient) for the inner plate is expected to be rather small (or high) compared to that of the outer plate. A much higher neutral fraction is redeposited on the inner divertor plate due to reaction chains associated with the charge exchange with plasma hydrogen ions and the electron-impact dissociative recombination of the resultant ions; these are the dominant reactions at low plasma temperatures (~1 eV).

As the dome wings do not face the plasma, deposition results from hydrocarbons eroded at the divertor plates through the divertor plasma as charge exchange neutrals and/or without being ionized. Fig. 3 shows asymmetric poloidal deposition of carbon/hydrocarbons between the inner and outer dome wings. The calculated distributions show the local deposition observed at the outer wing edge and the broad deposition on the entire inner

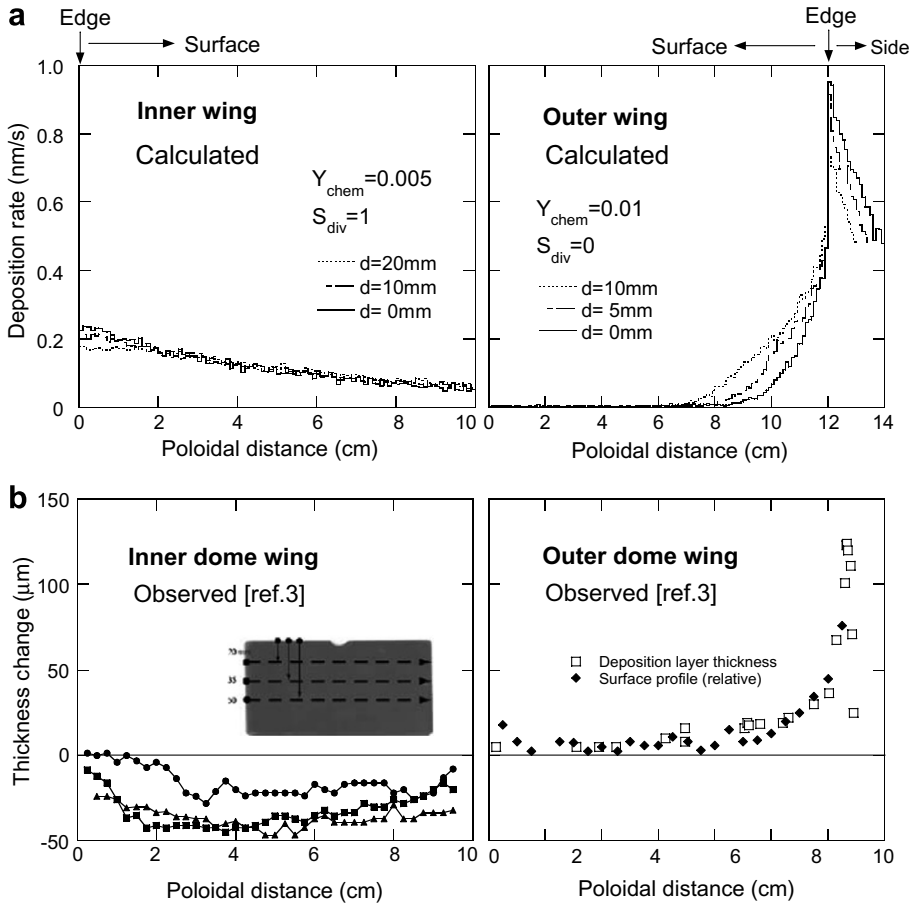

Fig. 3. Poloidal distribution of the number of redeposited particles on the inner and outer dome wings. (a) both the inner and outer divertor plates were bombarded by 10^8 plasma ions, and CH_4 molecules are released assuming chemical sputtering yields of 0.005 and 0.01 for the inner and outer divertor plates, respectively, and full and zero sticking, respectively, (b) shows variations in observed thickness on the inner and outer dome wings [10].

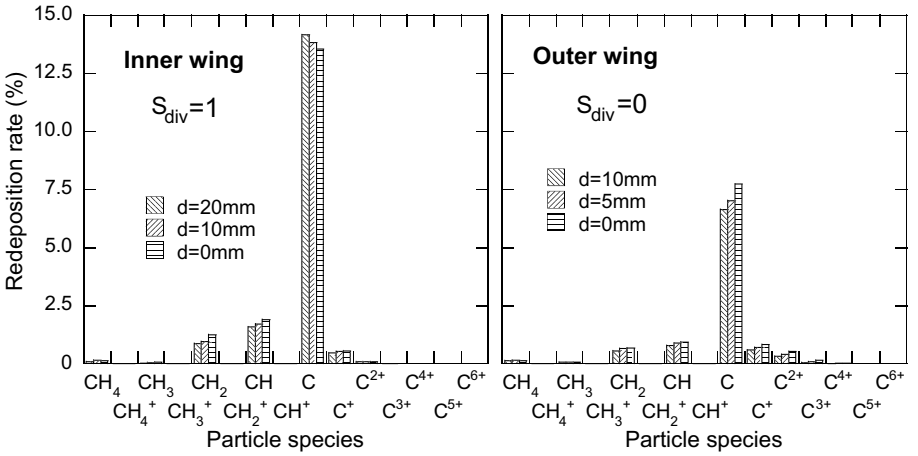

Fig. 4. Carbon and hydrocarbon species redeposited on the inner and outer dome wings. The divertor plates were bombarded by 10^8 plasma ions, and CH_4 molecules were released assuming chemical sputtering yields of 0.005 and 0.01 for the inner and outer divertor plates, respectively, and full and zero sticking, respectively.

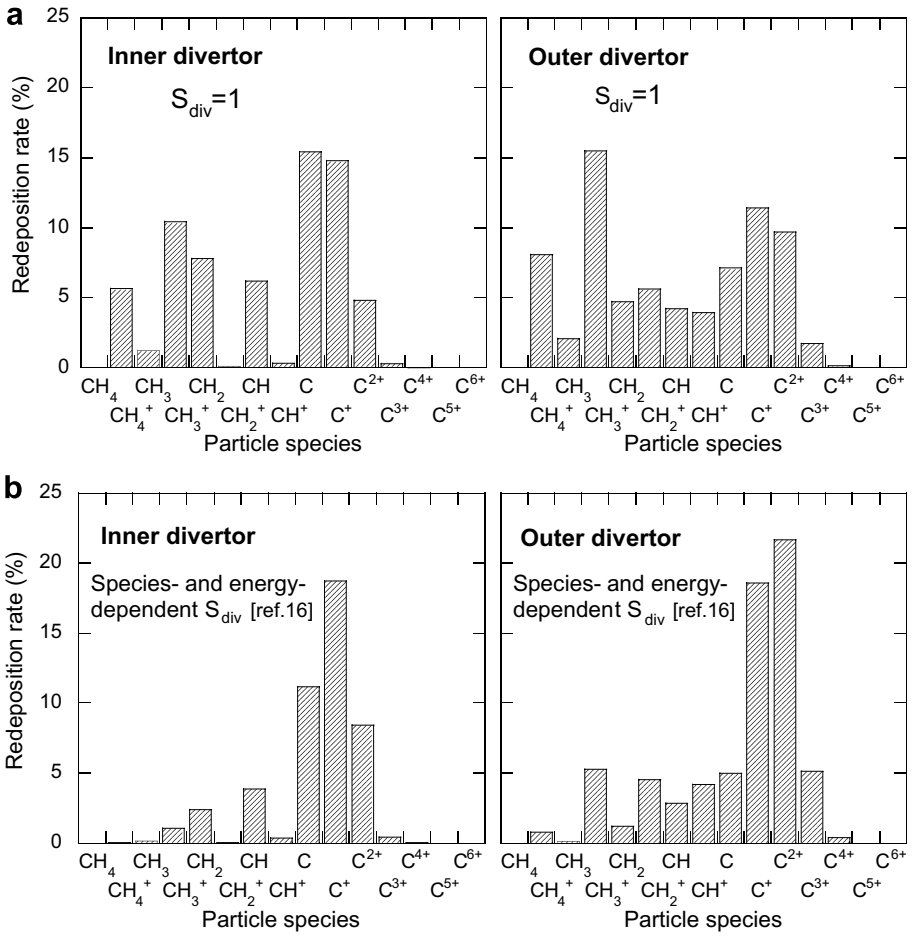

Fig. 5. Carbon and hydrocarbon species redeposited on the inner and outer divertor plates. The divertor plates were bombarded by 10^8 plasma ions, and CH_4 molecules were released. In (a), full sticking for all hydrocarbons on the plates was assumed. In (b), the energy- and species-dependent reflection coefficients [20] were used for the calculations.

dome wing. Assuming zero sticking on the diverter plates, 20% and 10% of hydrocarbons eroded from the divertor plates are deposited on the inner and outer dome wings, respectively. As shown in Fig. 4, the deposition species are mostly neutral carbon and hydrocarbons, which are dominant at low plasma temperatures (~1 eV). The neutral species liberated from the magnetic constraint are redeposited not only on the inner divertor plate but are also widely deposited on the inner dome wing. Accordingly, the thickness of the deposition layers on the inner dome wing decreases gradually toward the top of the dome. On the outer divertor plate, the ''neutral species are redeposited only at the bottom facing the low-temperature (< several eV) private plasma; heavy deposition appears at the bottom edge of the outer dome wing adjacent to the bottom of the outer divertor plate, while no deposition is recorded in the dome top. This provides a reasonable explanation of the local deposition observed on the outer dome wing (Fig. 3(b)), although the erosion observed on the inner dome wing is not explained by our calculations.

In general, although electron-impact ionization is the dominant process at high plasma temperatures, charge exchange with hydrogen ions and subsequent recombination with electrons is dominant at low plasma temperatures [19]. These reactions also dissociate the products and produce many different fragments. As shown in Fig. 5, the comparison of redeposition spectra between the inner and outer divertor plates is complex because of the plasma temperature distributions in front of the plates. Various neutral hydrocarbons and ions are deposited on the outer divertor plate, whereas fewer ion species are deposited on the inner plate. According to molecular dynamics simulation of the interactions between hydrocarbon molecules and the carbon surface [20], thermal-energy methane families have large reflection coefficient (small sticking); however, as the energy is increased, their reflection coefficient decreases and the incident hydrocarbon is fragmented into smaller molecules and atoms on the reflection. Therefore, the employment of the energy-dependent reflection coefficients for hydrocarbons and carbons enhances the deposition of carbon but suppress that of hydrocarbons.

4. Conclusions

The reasonable agreement obtained between the calculated and observed erosion distributions on the outer divertor plates was attained only on the assumption of negligible effective sticking of hydrocarbons on the outer divertor plate. Hydrocarbons released from the outer divertor plate were immediately ionized when entering the plasma and subsequently redeposited near the released positions; however, their small degree of effective sticking, i.e. re-erosion due to successive bombardments with plasma ions, results in long-range carbon transport. The observed thickness distribution of the carbon deposition layer on the inner divertor plate was dominated by the deposition of plasma carbon impurities with higher concentrations in the inner region than the outer region. Low plasma temperatures (~1 eV) in the inner divertor region result in the neutral hydrocarbon species liberated from the magnetic constraint being redeposited not only on the inner divertor plate but also on the inner dome wing. On the outer divertor plate, the neutral species are redeposited only on the bottom side facing the low-temperature private plasma; consequently, heavy deposition occurs at the bottom edge of the outer dome wing adjacent to the bottom of the outer divertor plate. This reproduces the observed local deposition on the outer dome wing that does not face the plasma; however, the observed erosion distribution on the inner dome wing is not explained by our calculations.

Acknowledgements

This work was undertaken as part of JAEA–Universities collaboration program. The support of a Grand-in-Aid for scientific research from the Ministry of Education, Culture, Sports, Science and Technology of Japan is was also gratefully acknowledged.

References

[1] D.G. Whyte, J.P. Coad, P. Franzen, H. Maier, Nucl. Fus. 39 (1999) 1025.
[2] J.P. Coad, P.L. Andrew, A.T. Peacick, Phys. Scr. T81 (1999) 7.
[3] J.P. Coad, N. Bekris, J.D. Elder, et al., J. Nucl. Mater. 290–293 (2001) 224.
[4] Y. Gotoh, J. Yagyu, K. Masaki, et al., J. Nucl. Mater. 313–316 (2003) 370.
[5] J.N. Brooks, Fus. Eng. Des. 60 (2002) 515.
[6] A. Kirschner, V. Philipps, J. Winter, U. Kögler, Nucl. Fus. 40 (2000) 989.
[7] J.N. Brooks, D. Alman, G. Federici, et al., J. Nucl. Mater. 266–269 (1999) 58.

[8] A. Kirschner, A. Huber, V. Philipps, et al., J. Nucl. Mater. 290–293 (2001) 238.
[9] A. Kirschner, V. Philipps, D.P. Coster, et al., J. Nucl. Mater. 337–339 (2005) 17.
[10] Y. Gotoh, T. Tanabe, Y. Ishimoto, et al., J. Nucl. Mater. 357 (2006) 138.
[11] H. Takenaga, T. Nakano, A. Asakura, et al., Nucl. Fus. S46 (2006) 39.
[12] K. Ohya, Phys. Scr. T124 (2006) 70.
[13] R.K. Janev, D. Reiter, Rep Forschungszentrum Jülich, Jül-3966, 2002.
[14] P.C. Stangeby, The Plasma Boundary of Magnetic Fusion Devices, IOP, Bristol, 2000, p. 296.
[15] K. Shimizu, H. Kubo, T. Takizuka, et al., J. Nucl. Mater. 220–222 (1995) 410.
[16] J.N. Brooks, Phys. Fluids B 2 (1990) 1858.
[17] T. Motohiro, Y. Taga, Thin Solid Films 112 (1984) 161.
[18] H. Kubo, JT-60 Team, Plasma Sci. Technol. 8 (2006) 50.
[19] K. Ohya, T. Tanabe, J. Kawata, Fus. Eng. Des. 81 (2006) 205.
[20] D.A. Alman, D.N. Ruzic, Phys. Scr. T111 (2004) 145.